

# One-Dimensional Earth-Abundant Nanomaterials for Water-Splitting Electrocatalysts

Jun Li and Gengfeng Zheng\*

Hydrogen fuel acquisition based on electrochemical or photoelectrochemical water splitting represents one of the most promising means for the fast increase of global energy need, capable of offering a clean and sustainable energy resource with zero carbon footprints in the environment. The key to the success of this goal is the realization of robust earth-abundant materials and cost-effective reaction processes that can catalyze both hydrogen evolution reaction (HER) and oxygen evolution reaction (OER), with high efficiency and stability. In the past decade, one-dimensional (1D) nanomaterials and nanostructures have been substantially investigated for their potential in serving as these electrocatalysts for reducing overpotentials and increasing catalytic activity, due to their high electrochemically active surface area, fast charge transport, efficient mass transport of reactant species, and effective release of gas produced. In this review, we summarize the recent progress in developing new 1D nanomaterials as catalysts for HER, OER, as well as bifunctional electrocatalysts for both half reactions. Different categories of earth-abundant materials including metal-based and metal-free catalysts are introduced, with their representative results presented. The challenges and perspectives in this field are also discussed.

not exist naturally. Different synthetic methods have been investigated to obtain hydrogen fuel, among which the most predominant approach used in industry today is to passing steam through hydrocarbons to produce  $H_2$  and  $CO_2$ .<sup>[6]</sup> The electrical water splitting represents  $\approx 4\%$  contribution of global hydrogen fuel production to date. Compared to other approaches, as the chemical reaction of water splitting is indeed the reverse reaction of hydrogen combustion, this process enables the complete and close cycle of hydrogen with zero carbon emission, and is thereby regarded as a substantially important and promising method.<sup>[8–14]</sup>

Firstly observed in 1789, the electrochemical water splitting is typically processed in an electrolyzer, which contains a cathode and an anode for the water reduction and oxidation half reactions, respectively.<sup>[1,5]</sup> An electrolyte is also used for transporting charges or ions between the cathode and anode. The overall chemical reaction is summarized as:  $H_2O \rightarrow H_2 + 1/2 O_2$ , although the two half reactions can be presented differently, depending on whether the reactions take place in acidic or neutral/basic electrolytes.<sup>[15]</sup> The water splitting reaction is an energy uphill process, and the standard-state free energy change ( $\Delta G^\circ$ ) for converting one mole of water molecules into hydrogen and oxygen gases is  $+237.2 \text{ kJ mol}^{-1}$ . When also taking the extra work for gas formation into consideration, the enthalpy change ( $\Delta H^\circ$ ) required is  $+286 \text{ kJ mol}^{-1}$  that accounts for 1 mol of  $H_2$  formation. The thermodynamic electrical potential for a reversible electrolysis cell voltage is  $1.23 \text{ V}$ .<sup>[6]</sup> Theoretically, when the applied potential across cathode and anode exceeds  $1.23 \text{ V}$ , the water reduction and oxidation take place, leading to the formation of hydrogen and oxygen gases that are released from the electrode surface. Nonetheless, in reality, an extra of voltage, known as the overpotential ( $\eta$ ), is always needed to apply for water splitting to proceed with reasonable reaction rates. An electrochemical reaction is often assessed by determining current flowing through an electrode as a function of applied potential (i.e., by recording  $i$ - $E$  curves).<sup>[16]</sup> The onset of the electrode (or cell) potential from the equilibrium value upon passage of faradaic current is known as polarization, which is regarded as the *overpotential*,  $\eta$ , a key parameter to evaluate electrocatalytic activity.

ical reaction is summarized as:  $H_2O \rightarrow H_2 + 1/2 O_2$ , although the two half reactions can be presented differently, depending on whether the reactions take place in acidic or neutral/basic electrolytes.<sup>[15]</sup> The water splitting reaction is an energy uphill process, and the standard-state free energy change ( $\Delta G^\circ$ ) for converting one mole of water molecules into hydrogen and oxygen gases is  $+237.2 \text{ kJ mol}^{-1}$ . When also taking the extra work for gas formation into consideration, the enthalpy change ( $\Delta H^\circ$ ) required is  $+286 \text{ kJ mol}^{-1}$  that accounts for 1 mol of  $H_2$  formation. The thermodynamic electrical potential for a reversible electrolysis cell voltage is  $1.23 \text{ V}$ .<sup>[6]</sup> Theoretically, when the applied potential across cathode and anode exceeds  $1.23 \text{ V}$ , the water reduction and oxidation take place, leading to the formation of hydrogen and oxygen gases that are released from the electrode surface. Nonetheless, in reality, an extra of voltage, known as the overpotential ( $\eta$ ), is always needed to apply for water splitting to proceed with reasonable reaction rates. An electrochemical reaction is often assessed by determining current flowing through an electrode as a function of applied potential (i.e., by recording  $i$ - $E$  curves).<sup>[16]</sup> The onset of the electrode (or cell) potential from the equilibrium value upon passage of faradaic current is known as polarization, which is regarded as the *overpotential*,  $\eta$ , a key parameter to evaluate electrocatalytic activity.

## 1. Introduction

With the fast consumption of fossil fuels and gradual deterioration of global climate and environment situations due to carbon release, the research and development of clean and sustainable energy resources such as solar and wind energies have the promise of satisfying the energy need with minimum carbon footprint in the environment.<sup>[1–5]</sup> Hydrogen has been well recognized as one of the most abundant and promising candidates for clean energy supply to replace fossil fuels since the beginning of 1970's, as the only combustion product is water.<sup>[6–13]</sup> Although hydrogen is one of the most abundant elements in the world, free hydrogen molecules do

J. Li, Prof. G. Zheng  
Laboratory of Advanced Materials  
Department of Chemistry  
Collaborative Innovation Center of Chemistry  
for Energy Materials  
Fudan University  
Shanghai 200433, China  
E-mail: gfzheng@fudan.edu.cn



This is an open access article under the terms of the Creative Commons Attribution License, which permits use, distribution and reproduction in any medium, provided the original work is properly cited.

DOI: 10.1002/advsc.201600380

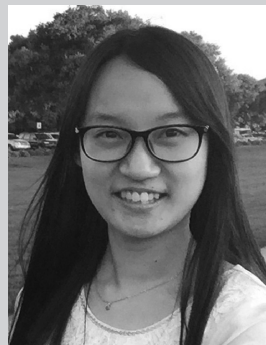
$$\eta = E - E_{eq} \quad (1)$$

Typically in the order of several hundred of millivolts, this overpotential enables the electron transfer process to overcome the high activation energy of kinetic barriers, which are accounted for the formation of reaction intermediates on the electrode surface.<sup>[17]</sup>

The overpotentials associated with the water reduction half-reaction (also known as hydrogen evolution reaction, HER) and the water oxidation half-reaction (also known as oxygen evolution reaction, OER) are plotted with corresponding current densities (Figure 1a, blue curves).<sup>[18]</sup> Their reversed reactions, that is, the oxygen reduction reaction (ORR) and hydrogen oxidation reaction (HOR) are also displayed in this plot for comparison (Figure 1a, orange curves).<sup>[18]</sup> The existence of overpotentials inevitably results in the cost of extra energy and lower conversion efficiency, and thereby catalysts are often used to incorporate on the electrode surface to reduce overpotential and increase the charge transfer towards water molecules. Generally, the electrocatalysts provide four main functions for water splitting: (i) stabilizing charge carriers (electrons and holes) and preventing them from recombination; (ii) offering adsorption sites for hydrogen and oxygen molecules; (iii) lowering the activation energies for water oxidation and reduction; and (iv) inhibiting the corrosion of the underlying semiconductor photoabsorbers. Thus, the major challenge in realizing hydrogen fuel for sustainable and clean energy conversion is the development of robust and scalable electrocatalysts, which allow for driving the electrochemical water splitting reactions with a high efficiency over a reasonably long period of time.

For the water reduction half-reaction (HER) in cathode, platinum (Pt) has still been widely used and regarded as the benchmark for the HER catalytic activity.<sup>[13]</sup> For the water oxidation half-reaction (OER) in anode, ruthenium (Ru) or iridium (Ir) based oxides have been mostly used with the best OER activities.<sup>[8]</sup> Nonetheless, as these noble metal-based materials are scarce and associated with high cost and limited sustainability, the large scale deployment of these catalysts are not feasible. In addition, compared to HER that is relatively kinetically favorable, the OER is much more sluggish and requires much higher overpotentials to drive the electrochemical reaction, which limits the overall water splitting efficiency and its wide applications. A similar challenge also exists for ORR<sup>[19,20]</sup> and its related applications like in fuel cells and metal-air batteries.<sup>[21,22]</sup> Moreover, most of the water splitting electrolyzers today are functioned in alkaline solutions, due to the general instability of metal oxides as OER catalysts in acidic conditions. Nonetheless, most of the HER catalysts (e.g. Pt and MoS<sub>2</sub>) have much better performances in acidic electrolytes. This mismatched pH condition inevitably reduces the device efficiencies and increases the fabrication cost.<sup>[23]</sup>

The research and development of earth-abundant materials for HER and OER electrocatalysts have attracted substantial interest in the past decade, with a variety of catalyst candidates being explored and developed. For the HER catalysts, transition metal sulfides, selenides, carbide, nitride, phosphide, and heteroatom-doped carbon have been reported.<sup>[15]</sup> For the OER catalysts, the effort of using earth-abundant catalysts has been mainly focused on three categories of materials:<sup>[18]</sup> Co, Ni, or Mn-based oxides, mixed oxides with spinel or perovskite structures, and Co, Ni-containing molecular complex or



**Jun Li** obtained her Bachelor degree (2016) at Fudan University in China, where she carried out undergraduate research with Prof. Gengfeng Zheng for nanomaterials-based energy conversion and storage. She was a recipient of several national undergraduate research awards including the Challenge Cup (2015)

and the Chinese Youth Innovation Award (2016), and several Fudan Undergraduate Research Opportunities Program (FDUROP) grants, including Deng-Hui program, Wang-Dao program, and Hui-Chun Chin and Tsung-Dao Lee Chinese Undergraduate Research Endowment. She is currently a graduate student in Department of Chemistry at Stanford University, USA.



**Gengfeng Zheng** obtained his Bachelor degree (2000) at Fudan University in China, and Master (2004) and PhD (2006) degrees in Chemistry at Harvard University in USA, under the guidance of Prof. Charles Lieber. He was a postdoctoral fellow working with Prof. Chad Mirkin at Northwestern University in USA (2007–2009). He became

a full professor in Department of Chemistry and Laboratory of Advanced Materials at Fudan University in 2010. His research interests include low-dimensional nanomaterial-based synthesis and surface chemistry, biosensing, biomaterial interface, photoelectrochemical conversion, electrocatalysis and energy storage.

macrocycles. In general, an ideal electrocatalyst should have the following features: (1) high efficiency that is similar to noble metal (oxide or hydroxide) based materials; (2) high chemical and catalytic activity over a wide range of pHs; (3) good durability with stable activity for a long time (months even years); (4) abundant sources and low cost; (5) environmental friendly; (6) scalability for commercial deployment; (7) potentials of integration for both HER and OER catalysts as well as integration with photoabsorbers like semiconductors.

The research of new electrocatalysts for water splitting has also been accompanied by the fast development of theoretical understanding of catalytic functions on the surface. Different parameters of materials in performing catalytic functions have been investigated, and summarized with their performances such as exchange current densities ( $j_0$ ). For instance, it has been proposed that the intrinsic activity of an HER catalyst is well

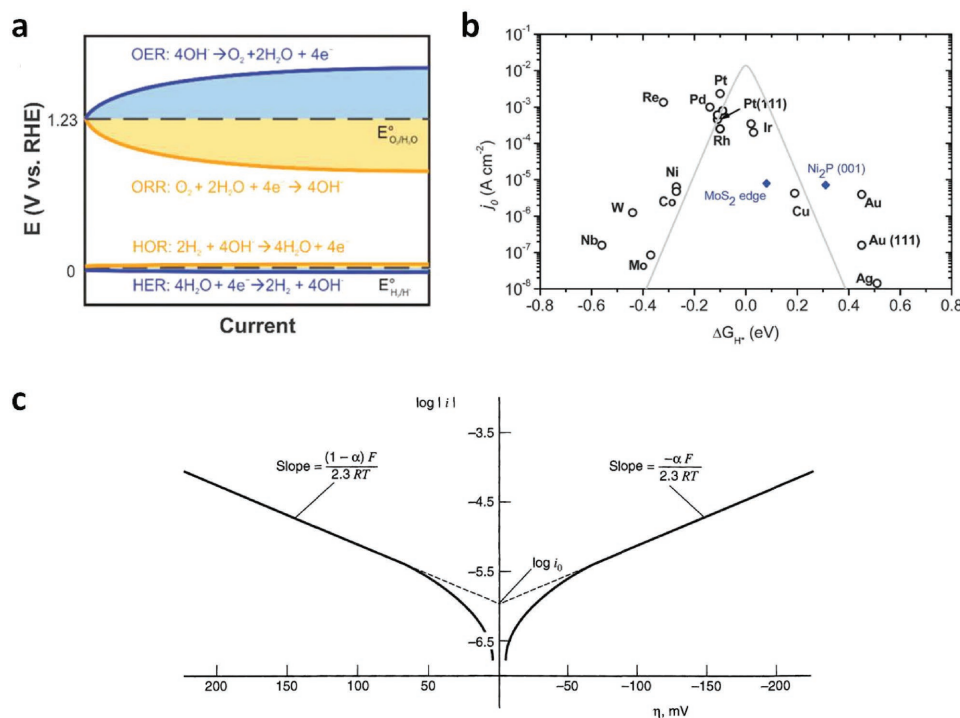


**Figure 1.** a) Schematic of the overpotentials associated with oxygen electrocatalysis (OER, ORR) and hydrogen electrocatalysis (HER, HOR). Reproduced with permission.<sup>[18]</sup> Copyright 2015, Royal Society of Chemistry. b) A volcano plot of experimentally measured exchange current density as a function of the DFT-calculated Gibbs free energy of adsorbed atomic hydrogen. Reproduced with permission.<sup>[6]</sup> Copyright 2014, Royal Society of Chemistry. c) Tafel plots for anodic and cathodic branches of the current-overpotential curve, with  $\alpha = 0.5$ ,  $T = 298$  K, and  $j_0 = 10^{-6}$  A cm<sup>-2</sup>. Reproduced with permission.<sup>[16]</sup>

correlated with the Gibbs free energy for hydrogen adsorption ( $\Delta G_{\text{H}^*}$ ) on a catalyst surface.<sup>[24]</sup> For OER, one universal parameter is the difference between the adsorption free energies change between reaction intermediates of O\* and OH\* (i.e.,  $\Delta E_{\text{O}^*} - \Delta E_{\text{OH}^*}$ ).<sup>[18]</sup> By plotting the exchange current density of different materials with those structural parameters such as  $\Delta G_{\text{H}^*}$ , a triangular shape can be observed and is known as the volcano plot (Figure 1b), which indicates that both the weak and strong interactions between the reactant species and the catalyst surface are not favorable for the optimal catalytic activity. Thus, for an ideal catalyst, the system needs to attain to the top of the activity volcano plot, which should be observed experimentally with the highest value of the exchange current density. For example, it can be seen that Pt group metals are in the top of the HER volcano.

In addition to the catalyst material selection, the design and fabrication of nanostructured electrocatalysts have been driving a significant increase of efficiency in the past decade, either by preferentially exposing high-index facets or active reaction sites, and/or electrically connecting these sites for fast charge transport/transfer. Thus, the morphology and structure of the designed catalysts can also provide significant benefits for their performances.<sup>[6,25]</sup> Among different types of morphologies and structures, the one-dimensional (1D) nanoscale materials have been demonstrated as one unique target for serving excellent electrocatalyst candidates (Figure 2).<sup>[26–28]</sup> First, these 1D materials have high surface areas, large roughness factors and high active-site densities, which are beneficial for providing

efficient catalytic activity for surface electrochemical reactions. Second, the 1D materials can provide channels and few crystal boundaries for fast charge transport pathways with reduced scattering. Third, the existence of abundant open space and porosity between adjacent 1D nanostructures enables fast mass transport and chemical accessibility of electrolyte molecules into the deep portion of the electrode/catalyst surface. Fourth, the 1D materials can be directly grown and contacted on the underlying electrode surface, and thus provide efficient charge transport with low contact resistance, as well as waive the need of adding conducting additives or binders. Fifth, the formation

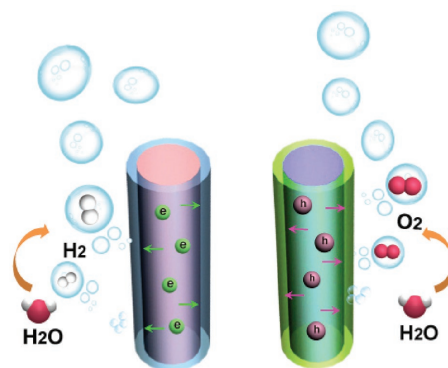


**Figure 2.** Scheme of benefits for one-dimensional nanoscale materials as one unique target for serving excellent electrocatalyst candidates.

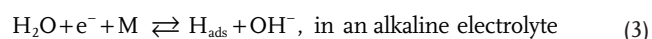
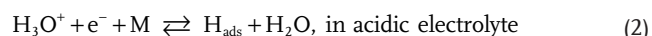
and release of bubbles can also be facilitated from the 1D nanomaterial electrode/catalyst surface, thus preventing the bubbles blocking of subsequent reaction process.

The 1D nanomaterials have been discovered and become prosperous in the past two decades. Substantially research efforts have been invested into the synthesis of these 1D materials, which allow for exquisite controls of composition, morphology, heterostructures, and reactivity.<sup>[28,29]</sup> The capability of modulation the composition and doping, either radially or even longitudinally, even within a single 1D nanostructure has been explicitly demonstrated.<sup>[30,31]</sup> Thus, these achievements have also brought substantial advances and breakthroughs in the applications of utilization of 1D materials in almost all fields of modern technologies,<sup>[29,32–34]</sup> including the water splitting electrocatalysts.

In the following sections, we will first describe the representative progresses in studying 1D materials for HER and OER catalysts, respectively, with their representative examples including metal-based and metal-free materials illustrated. Then we will discuss the recent development of bifunctional HER/OER electrocatalysts for both water reduction and oxidation simultaneously. Finally, we will summarize these studies of electrocatalyst materials and structures, and suggest the challenges and future perspectives in this field.

## 2. HER

The mechanism of the HER process has been extensively studied in past decades, which can be divided into two steps.<sup>[35]</sup> The first step is known as Volmer reaction, in which a proton adsorption on an empty active site of the electrode is coupled with an electron transfer, and yields an adsorbed hydrogen ( $H_{ads}$ ). In acidic or alkaline solutions, the proton source is the hydronium ion or a water molecule, respectively.<sup>[15]</sup>



For the second step, two different pathways may occur. One is Heyrovský reaction, in which a  $H_2$  molecule is formed by combination of the  $H_{ads}$  on the catalyst surface, an electron and another proton (e.g.  $H_3O^+$  ion), followed by desorption from the catalyst surface:



The other pathway is Tafel reaction, in which a  $H_2$  molecule is formed by directly combining two  $H_{ads}$  and desorbs from the catalyst surface. This pathway has been confirmed in the case of Pt.



Early works of this pathway indicated that the current is often correlated exponentially to the overpotential  $\eta$ . Given by Tafel in 1905,<sup>[16]</sup>

$$\eta = a + b \log i \quad (6)$$

A model of electrode kinetics should explain the validity of the equation above, which is known as the Tafel equation.

A Tafel plot, i.e., a plot of  $\log i$  vs.  $\eta$ , is indispensable for estimating kinetic parameters. In general, there is an anodic branch with a slope of  $(1-\alpha)F/2.3RT$  and a cathodic branch with a slope of  $-\alpha F/2.3RT$ . As shown in Figure 1c,<sup>[16]</sup> both linear segments are extrapolated to an intercept of  $\log i_0$ . The plots apparently deviate from linear behavior as  $\eta$  approaches zero, as the backward reactions can no longer be regarded as negligible. The transfer coefficient,  $\alpha$ , and the exchange current,  $i_0$ , are readily accessible from this presentation, when it can be applied. The Tafel slope, indicating the potential difference for altering the current density by 10-fold, is often used to investigate which pathway it is involved during the HER process.

In spite of its scarcity and high cost, Pt has still been the most widely used and the state-of-the-art catalyst for HER, especially in acidic conditions.<sup>[13]</sup> A number of earth-abundant materials have also been reported in the past decade for HER catalysts, which are almost exclusively from the transition metal elements of Co, Ni, Mo, W, Fe and Cu, and nonmetal elements of B, C, N, O, S and Se.<sup>[15]</sup> The abundance order of these transition metal elements in the earth crust is given as:  $W = Mo < Co < Cu < Ni \ll Fe$ .<sup>[15]</sup> Thus, the capability of utilizing these non-precious metal elements, especially Fe and Ni, should be substantially important for developing large-scale water splitting technologies. To date, a wide variety of noble-metal-free HER catalysts have been explored and reported for water reduction half-reaction, including transition metals and their compounds (such as sulfides, selenides, nitrides, carbides, oxides and hydroxides), nanocarbon and their inherited composites, natural hydrogenases and artificial organometallic molecules. In this work, we will focus our discussion on those materials with 1D morphologies. Other comprehensive reviews on HER electrocatalysts can be found elsewhere.<sup>[6,8,11,12,15,36]</sup>

### 2.1. Metal-Based 1D Nanomaterials

In 2014, Sun and coworkers developed a topotactic conversion method to directly grow self-supported nanoporous cobalt phosphide nanowire arrays on carbon cloth (designated as CoP/CC) via phosphidation of their  $Co(OH)F$  precursor.<sup>[37]</sup> This CoP/CC nanowire array was demonstrated as a hydrogen-evolving cathode for a wide range of pH from 0 to 14 with good stability. In the acidic condition, a low onset overpotential (38 mV) and a small Tafel slope (51 mV  $dec^{-1}$ ) were obtained. In the neutral and basic conditions, the onset potentials were 45 and  $\approx 80$  mV, and the Tafel slopes were 93 and 129 mV  $dec^{-1}$ , respectively. The same research group also reported the synthesis of FeP nanowire array supported on Ti plate from its precursor,<sup>[38]</sup> and the synthesis of self-supported  $Cu_3P$  nanowire arrays on porous copper foam.<sup>[39]</sup> In these demonstrations, the non-noble metal phosphides were synthesized by a similar low-temperature phosphidation reaction from their corresponding (oxy)hydroxide precursors, such as  $\beta$ -FeOOH and  $Cu(OH)_2$ . A conducting substrate, such as carbon cloth, Ti plate or Cu foam, was used as the current collector to expedite the charge transport. Later, it was also found that in addition to the electrocatalytic activity, the CoP nanowire arrays also functioned as semiconductor with visible-light absorption, enabling photocatalytic evolution of hydrogen

from water under visible light.<sup>[40]</sup> A hole-capturing reagent, triethanolamine (TEOA) was used as a sacrificial agent. During 40 min of continuous visible-light irradiation, the amount of H<sub>2</sub> gas evolved was 66.1 μmol for the CoP nanowire arrays, while this value was increased to 160.7 μmol when a dye molecule, P<sub>HIV</sub>, was pre-linked to the CoP nanowire surface. This was the first example of using CoP for photocatalytic hydrogen generation.<sup>[40]</sup>

The effect of different morphologies on their catalytic activities has also been studied for a variety of earth-abundant HER electrocatalysts, such as MoS<sub>2</sub>,<sup>[41–43]</sup> amorphous MoS<sub>2</sub>,<sup>[44]</sup> WS<sub>2</sub>,<sup>[45,46]</sup> Ni<sub>2</sub>P,<sup>[47]</sup> CoP<sup>[48]</sup> and Ni-Mo alloys.<sup>[49,50]</sup> In 2014, Jin and coworkers reported the synthesis of metallic cobalt pyrite (cobalt disulfide, CoS<sub>2</sub>) with different morphologies including films, microwires and nanowires, and showed their capabilities as a high-activity candidate for HER.<sup>[27]</sup> In contrast to other semiconducting pyrites like NiS<sub>2</sub> or FeS<sub>2</sub>, CoS<sub>2</sub> has a high intrinsic conductivity with a sheet resistance of ≈ 19.2 Ω sq<sup>-1</sup>, thus making it a promising electrocatalytic material. This stable and metallic feature of CoS<sub>2</sub> is also more advantageous than other layered transition metal dichalcogenide electrocatalysts like MoS<sub>2</sub> and WS<sub>2</sub>, which can only show high HER activity after conversion from the thermodynamically stable semiconducting phase to a metastable metallic polymorph.<sup>[27]</sup> Different CoS<sub>2</sub> morphologies were formed from thermal sulfidation of corresponding Co(OH)<sub>2</sub> precursors and used for HER.<sup>[27]</sup> It was clear that the morphologies of CoS<sub>2</sub> catalysts played an important role for their HER performances, which were substantially boosted with the increase of effective electrode surface areas for microwires and nanowires (Figure 3a). For CoS<sub>2</sub> nanowires, a geometric current density of ~10 mA cm<sup>-2</sup> was obtained at an overpotential as low as ~145 mV vs. reversible hydrogen electrode (RHE) (Figure 3b). In addition, both the micro- and nanowires provided a synergistic effect by enhancing the evolution of gas bubble from the electrode surface. With CoS<sub>2</sub> films, large bubbles tended to be trapped at the electrode surface, thus reducing the catalytically-active sites.<sup>[27]</sup> In contrast, the 1D micro- and nanostructures provide high surface area and large surface curvature, air bubbles

attached to these 1D micro- and nanostructures have much higher surface energy, and thus tend to be released from the surface. This phenomenon is similar to air bubbles at the microstructured surface of a lotus leaf.<sup>[51]</sup> As a result, more rapid liberation of catalytically-active sites is achieved by faster release of bubble, thus benefiting for further contact of electrolytes on the catalyst/electrode surface. Later, the same research group reported a type of ternary pyrite-type cobalt phosphosulphide (CoPS) nanowires as a highly efficient catalyst for both electrochemical and photoelectrochemical hydrogen evolution.<sup>[52]</sup> By combining with a theoretical study, it was shown that the CoPS nanowire electrodes presented a geometrical current density of 10 mA cm<sup>-2</sup> at a low overpotential of 48 mV vs. RHE. When integrated with n<sup>+</sup>-p-p<sup>+</sup> silicon micropylramids for photoabsorption and conversion, this hybrid catalyst/electrode enabled a photocurrent density of 35 mA cm<sup>-2</sup> at 0 V vs. RHE, and onset photovoltages as high as 450 mV vs. RHE, which marked the most efficient solar-driven hydrogen generation from earth-abundant materials.

By a similar design concept, our group demonstrated the conversion of spinel-type nickel cobalt oxide (NiCo<sub>2</sub>O<sub>4</sub>) nanowires into pyrite-type nickel cobalt sulfide (Ni<sub>0.33</sub>Co<sub>0.67</sub>S<sub>2</sub>) nanowires, via a thermal sulfidation process.<sup>[35]</sup> The obtained Ni<sub>0.33</sub>Co<sub>0.67</sub>S<sub>2</sub> nanowires presented 1D morphology and expedited charge transport capability, and thus served as a stable and efficient HER catalyst for a wide pH range. Under the acidic, neutral and basic electrolytes, the onset potentials were measured as low as -65, -39 and -50 mV vs. RHE, and Tafel slopes were 44, 68 and 118 mV dec<sup>-1</sup>, respectively, which were much better than individual CoS<sub>2</sub> or NiS<sub>2</sub> nanostructures under similar conditions. In addition to phosphides and sulfides, carbides have also been synthesized in 1D structures for HER.<sup>[53]</sup> For example, nanoporous Mo<sub>2</sub>C nanowire arrays were synthesized by pyrolysis of a MoO<sub>x</sub>/amine hybrid precursor under an inert atmosphere.<sup>[54]</sup> Due to the close contact of MoO<sub>x</sub> and amine molecules, a quasi-homogeneous reaction environment was created, which facilitated the formation of nanocrystallites, abundant nanoporosity, and large active surface area, thus leading to excellent HER activity.

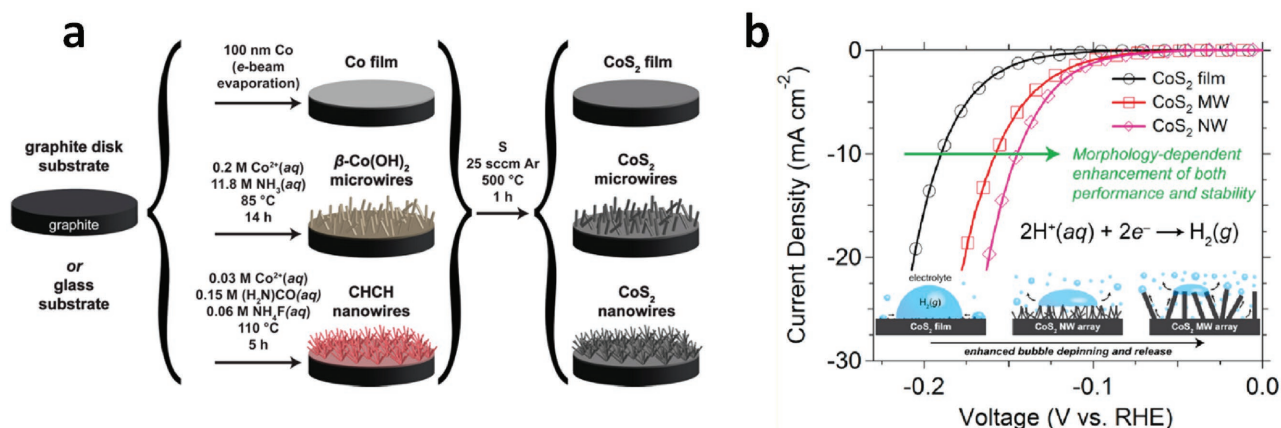


**Figure 3.** a) Schematic depictions of the preparation of a cobalt pyrite (CoS<sub>2</sub>) film, microwire array, or nanowire array on a graphite disk substrate. b) Electrochemical characterization of CoS<sub>2</sub> film, microwire (MW) array, and nanowire (NW) array electrodes for HER electrocatalysis. Reproduced with permission.<sup>[27]</sup> Copyright 2014, American Chemical Society.

## 2.2. Incorporation of Metal-Based Nanomaterials on 1D Substrates

The direct growth or attachment of the effect metal phosphides, sulfides, carbides or selenides onto nanoscale structure surface has also been regarded as an important approach for making the 1D catalyst/electrode interface. Among many nanostructured electrode candidates, carbon nanotubes (CNTs) are the most recognized one, due to their convenient and large-scale synthesis, high intrinsic conductivity and environmental benignity.<sup>[55]</sup> Nitrogen doping has also been interrogated to further increase the conductivity and electrocatalytic activity of CNTs, due to the comparatively higher electron negativity of nitrogen atoms than carbon.<sup>[12]</sup> In 2014, Dai and coworkers reported the formation of nanoscale NiO/Ni heterostructures on the CNT sidewalls as an active and stable HER catalyst.<sup>[56]</sup> The NiO/Ni heterostructure was fabricated serendipitously by thermal annealing, resulting in partially reduced Ni(OH)<sub>2</sub> nanoparticles. The CNTs were partially oxidized and impeded the complete reduction and Ostwald ripening of Ni species into the less HER active Ni phase (Figure 4a). Compared to NiO/CNT and Ni/CNT samples, the NiO/Ni-CNT catalyst exhibited a clearly better HER activity with a lower overpotential and a higher current density (Figure 4b), thus indicating a synergistic effect between NiO and Ni. The electrocatalytic activity was close to that of Pt under similar conditions. When this NiO/Ni-CNT was coupled with a NiFe-layered double hydroxide (NiFe LDH) water oxidation catalyst and used as cathode and anode, respectively, the water electrolyzer achieved a current density of 20 mA cm<sup>-2</sup> at an applied potential of 1.5 V by a single-cell AAA alkaline battery (Figure 4c).

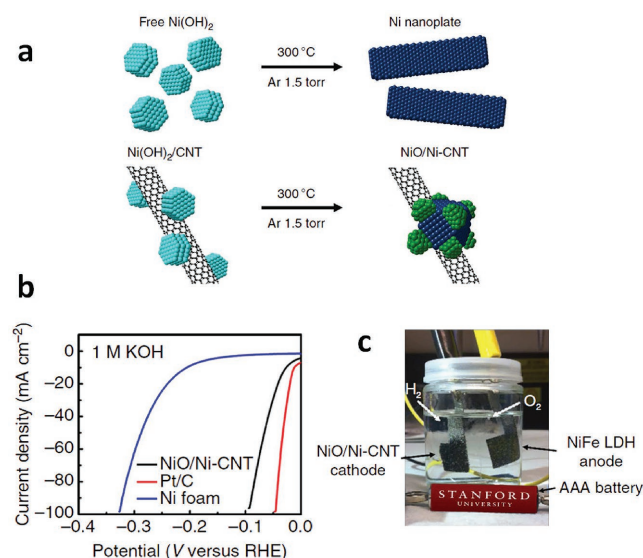


**Figure 4.** a) Schematic illustration of the structural difference between CNT hybrid and pure nanoparticle. b) Linear sweep voltammetry of NiO/Ni-CNT, Pt/C deposited on Ni foam and pure Ni foam at a scan rate of 1 mV s<sup>-1</sup> under the loading of 8 mg cm<sup>-2</sup> in 1 M KOH. c) Demonstration of water-splitting device powered by an AAA battery with a nominal voltage of 1.5 V. Reproduced with permission.<sup>[56]</sup> Copyright 2014, Nature Publishing Group.

In addition to Ni, the Co-based, Mo-based and Fe-based materials have also been investigated by incorporating on the surface of CNTs. In 2014, Asefa and coworkers reported the synthesis of Co-embedded, nitrogen-doped CNTs, using a thermal treatment of Co<sup>2+</sup>-incubated CNTs from inexpensive dicyandiamide and CoCl<sub>2</sub> as starting materials.<sup>[57]</sup> It was found that these Co-embedded N-doped CNTs functioned well under acidic, neutral or basic electrolytes with a HER activity close to Pt. Structural analysis revealed that this good activity was mainly attributed to the nitrogen dopants and concomitant structural defects. Similarly, amorphous molybdenum sulfide (MoS<sub>x</sub>) layer (≈2 nm thick) was formed by decomposition of precursors onto N-doped CNT forest surface.<sup>[58]</sup> An onset potential of 75 mV and a small overpotential of 110 mV for a current density of 10 mA cm<sup>-2</sup> were achieved, which represented the highest HER performance for MoS<sub>x</sub>-based materials at that time. Deng et al. developed a method of encapsulating Fe, Co and Fe/Co alloy into nitrogen-doped CNTs by using a chemical vapor deposition (CVD) approach,<sup>[59]</sup> which exhibited an excellent stability and a high activity with ≈70 mV onset overpotential vs. RHE, close to that of commercial 40% Pt/C catalyst. In another study, using dicyandiamine as precursor and Co<sub>3</sub>O<sub>4</sub> nanowire array as catalyst, the Sun group reported the direct chemical vapor deposition (CVD) synthesis of a film of interconnected Co-entrapped, nitrogen-doped CNTs on carbon cloth.<sup>[60]</sup> The dense CNT networks provided a high catalyst loading and strong coupling of the catalyst, and the obtained catalyst showed a high hydrogen-evolving activity and durability over the whole pH range.

Similar to the aforementioned conversion of free-standing oxides or (oxy)hydroxides, the in situ conversion of these materials grown on CNTs into corresponding sulfides, phosphides, and so on, can also be processed in a similar manner. For instance, CoP nanocrystals decorated on CNTs were synthesized by the low-temperature phosphidation of a Co<sub>3</sub>O<sub>4</sub>/CNT precursor.<sup>[61]</sup> Co-doped iron pyrite nanosheets were interfaced with CNTs (Fe<sub>1-x</sub>Co<sub>x</sub>S<sub>2</sub>/CNT hybrid) by solution reaction of Fe salt, Co salt and thioacetamide, followed by thermal treatment.<sup>[62]</sup> A strong dependence of the Co doping ratio on the HER activity of the Fe<sub>1-x</sub>Co<sub>x</sub>S<sub>2</sub>/CNT hybrid catalyst was found. For 10% of Co doping with a high catalyst loading (≈7 mg cm<sup>-2</sup>), the Fe<sub>0.9</sub>Co<sub>0.1</sub>S<sub>2</sub>/CNT hybrid presented a lowest overpotential of ≈0.12 V at a current density of 20 mA cm<sup>-2</sup>, and a Tafel slope of 46 mV dec<sup>-1</sup>.

## 2.3. Metal-Free 1D Carbonaceous Nanomaterials

In spite of these progresses, the use of metal ions in these catalysts still encounters the possibility of metal ion dissolution and release, thereby reducing the catalytic activity and increasing the environmental impact. The development of metal-free catalysts has also become an important focus recently, mainly for the carbon-based materials. For instance, it was first reported in 2014 that pristine CNTs were active by acidic oxidation to achieve enhanced electrochemical reduction capability of converting protons to hydrogen,<sup>[63]</sup> although the strong acidic oxidation may also deteriorate the electrical conductivity and the catalytic activity. Likewise, carbon nitride (C<sub>3</sub>N<sub>4</sub>) can also be synthesized to show similar HER catalytic activity. For

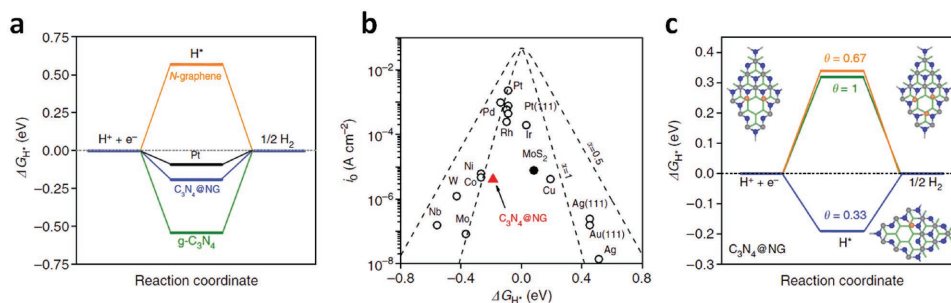
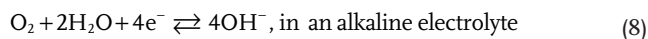
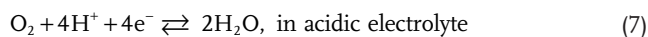


**Figure 5.** a) The calculated free-energy diagram of HER at the equilibrium potential for three metal-free catalysts and Pt reference. b) Volcano plots of exchange current density as a function of the  $\Delta G_{H^*}$  for newly developed  $C_3N_4@NG$  (red triangle), common metal catalysts as well as a typical nanostructured  $MoS_2$  catalyst. c) Free-energy diagram of HER on the surface of  $C_3N_4@NG$  under different  $H^*$  coverage (1/3, 2/3 and 1 with the molecular configurations shown as insets) conditions. Reproduced with permission.<sup>[65]</sup> Copyright 2014, Nature Publishing Group.

example, using the hydrogen-bonded cyanuric acid melamine supramolecular complex as precursor, 1D  $C_3N_4$  nanorod were synthesized on a variety of different substrates, due to the interaction of free hydroxyl and amine groups of the supramolecular complex precursor.<sup>[64]</sup> One early bench mark progress in this field was reported by the Qiao group, who reported the preparation of graphitic- $C_3N_4$  coupled with N-doped graphene ( $C_3N_4@NG$ ).<sup>[65]</sup> This metal-free hybrid catalyst exhibited an unexpectedly high HER activity that was comparable to some of the well-developed metallic catalyst. Density functional theory calculations showed that the free-energy changes of  $H^*$  adsorption and  $H_2$  desorption from  $C_3N_4@NG$  was closer to the level of Pt than those of N-doped graphene and graphitic- $C_3N_4$  (Figure 5a). The  $\Delta G_{H^*}$  of the developed  $C_3N_4@NG$  was also plotted together with common metal catalysts in the volcano plot (Figure 5b), and the free energy diagram for different surface coverage of  $H^*$  on  $C_3N_4@NG$  was also calculated (Figure 5c). Together with the experimental approaches, this study revealed that the unconventional electrocatalytic property was originated from an intrinsic chemical and electronic coupling, which synergistically enhanced the proton adsorption and reduction kinetics. Furthermore, theoretical approaches have robustly been used to interrogate the mechanism of the metal-free catalytic process, which revealed that the Volmer-Heyrovsky step is the predominant HER mechanism while the Heyrovsky step is the rate-determining for CNTs.<sup>[66,67]</sup>

### 3. OER

Likewise, the oxygen evolution can take place in either acidic or alkaline conditions, with the corresponding half reactions as:



This 4-electron half-reaction involves multiple reaction intermediates (i.e.,  $OOH^*$ ,  $O^*$  and  $OH^*$ ) in the mechanism, either in acidic or alkaline conditions.<sup>[18]</sup> Compared to HER, the water oxidation half-reaction (OER) is much more sluggish in kinetics. Generally, it is believed that the mechanism is attributed to the interaction of oxygen atom with the  $d$ -electrons of the transition

metal ions.<sup>[8,18]</sup> The best reported OER performances are still marked by the noble metal oxides such as  $RuO_2$  and  $IrO_2$ , with overpotentials of as low as 140 mV for  $RuO_2$  in alkaline conditions.<sup>[68,69]</sup> To date, for earth-abundant metal-based materials, most of the non-noble-metal oxides and hydroxides reported for OER catalysts are focused on those of Co, Ni, Mn, Fe, Mo and W.<sup>[8,18,70]</sup>

#### 3.1. Metal-based 1D Nanomaterials

It has been long known that  $Co_3O_4$  is an ideal OER catalyst with high efficiency and good corrosion stability,<sup>[71]</sup> but previous studies of these Co-based oxides for OER were predominantly in the form of thin films or agglomerated particles. One of the earliest examples of using 1D  $Co_3O_4$  nanowires for OER was reported in 2010,<sup>[26]</sup> in which the synthesis of mesoporous  $Ni_xCo_{3-x}O_4$  nanowire arrays was first achieved on the surface of Ti foils via an ammonia evaporation induced growth. Spectroscopic characterizations indicated that the Ni element had an uneven distribution and was concentrated on the nanowire surface. Compared to  $Co_3O_4$  nanowires without Ni doping, this Ni doping allowed for the enhancement of the OER activity, with enhanced electrical conductivity and double layer capacitance. Other elemental dopings of the  $Co_3O_4$  have also been reported. For instance, by co-deposition of both Zn and Co molecular precursors on Ti foils followed by thermal conversion, 1D  $Zn_xCo_{3-x}O_4$  branched nanostructures were constructed with small secondary nanoneedles directly grown from primary rhombus-shaped nanopillar arrays.<sup>[72]</sup> A small overpotential of  $\approx 0.32$  V was required for this  $Zn_xCo_{3-x}O_4$  nanostructure to achieve  $10 \text{ mA cm}^{-2}$ , with a Tafel slope of  $51 \text{ mV dec}^{-1}$ , substantially exceeding those of pristine  $Co_3O_4$  NWs.

Besides elemental doping, the tuning of the oxygen vacancies of those oxides has also been demonstrated as an effective means, as the oxygen vacancies are known as the charge carriers of many oxides such as  $Co_3O_4$ .<sup>[73]</sup> Previously, the thermal annealing in a reducing environment such as hydrogen gas was demonstrated to enhance the electrical performances of  $TiO_2$  and other metal oxides,<sup>[74–76]</sup> while this hydrogen annealing is not energy efficient or safe, and not applicable especially for the thermally instable materials. In 2014, our group reported a mild, solution-based approach to chemically reduce  $Co_3O_4$

nanowires into their reducing forms with  $\text{NaBH}_4$ .<sup>[73]</sup> In that work, mesoporous  $\text{Co}_3\text{O}_4$  nanowires were first synthesized with a surface area of  $58 \text{ m}^2 \text{ g}^{-1}$  and a mean mesopore size of 6–8 nm. Afterwards, these nanowires were reduced in a  $\text{NaBH}_4$  solution at room temperature. Although no significant differences in the morphology or structure were observed, the spectroscopic measurements indicated the increase of oxygen vacancies inside the pristine  $\text{Co}_3\text{O}_4$  crystal structures. Compared to the pristine counterparts, the chemically reduced  $\text{Co}_3\text{O}_4$  nanowires presented a much lower onset potential of 1.52 vs. RHE, and a much larger current density of  $13.1 \text{ mA cm}^{-2}$  at 1.65 V vs. RHE. Density functional theory calculations suggested that the existence of oxygen vacancies inside these oxides result in the formation of new gap states, where the electrons previously associated with the Co-O bonds tend to be delocalized, leading to much higher OER activity.<sup>[73]</sup>

In addition to Co-based oxides and (oxy)hydroxides, other transition metal compounds have also been developed for OER. For instance, manganese oxides with different structures, including  $\alpha$ -,  $\beta$ -,  $\delta$ - $\text{MnO}_2$  and amorphous were synthesized and compared.<sup>[77]</sup> The structures of different  $\text{MnO}_2$  depend on the connectivity between the  $[\text{MnO}_6]$  units via sharing corners or edges, with  $\delta$ - $\text{MnO}_2$  as layered structures and  $\alpha$ -,  $\beta$ - $\text{MnO}_2$  as 1D structures. It was found that the OER activity of these  $\text{MnO}_2$  catalysts in an alkaline media was strongly dependent on the crystallographic structures, with an order of  $\alpha$ - $\text{MnO}_2 > \text{amorphous} > \beta$ - $\text{MnO}_2 > \delta$ - $\text{MnO}_2$ . An overpotential of 450 mV was required for  $\alpha$ - $\text{MnO}_2$  to present a current density of  $10 \text{ mA cm}^{-2}$ , compared to a 380 mV overpotential required by an Ir/C catalyst. Meanwhile, at a constant current density of  $5 \text{ mA cm}^{-2}$ , a 3-h stability was achieved by  $\alpha$ - $\text{MnO}_2$ , which was further extended to  $\approx 8 \text{ h}$  when adding with Ni dopants. In another example, Zhang and coworkers reported the synthesis of  $\text{Ni}_3\text{S}_2$  nanorods on Ni foam by a simple hydrothermal reaction.<sup>[70]</sup> Spectroscopic measurements revealed that rich and unconventional oxidation states of Ni ( $\text{Ni}^0$ ,  $\text{Ni}^+$  and  $\text{Ni}^{2+}$ ) existed in the  $\text{Ni}_3\text{S}_2/\text{Ni}$  composite, owing to the synergetic chemical coupling effects among  $\text{Ni}_3\text{S}_2$  nanorods, NiO layer and the Ni foam support, thus leading to an ultra-low overpotential. In a 0.1 M KOH solution, an overpotential of as low as  $\approx 187 \text{ mV}$  was required to achieve a current density of  $10 \text{ mA cm}^{-2}$ , much lower than that of other transition metal oxides or 20 wt% Pt/C. This value was also comparable to that of  $\text{RuO}_2$ , marking the best OER performance among the non-noble metal inorganic electrocatalyst at that time.

Although 1D nanostructures provide efficient charge transport channels and abundant space between their neighbors, the surface areas of pristine 1D nanostructures

may still be lower compared to 0- or 2-dimensional nanomaterials. Inspired by the heterostructure of plant leaves, our group developed a 2D/1D  $\text{CoO}_x$  heterostructure by a solution-based cation exchange process, which was composed by ultrathin  $\text{CoO}_x$  nanosheets that were further assembled into a nanotube structure.<sup>[78]</sup> This 2D/1D  $\text{CoO}_x$  heterostructure enabled the optimization of structure and OER activity over different length scales (Figure 6a). At the atomic scale, the  $\text{Co}^{2+}$  presented an octahedral electronic structure that is beneficial for OER. At the nanoscale, the self-assembly of high-density, ultrathin  $\text{CoO}_x$  nanosheets precluded the aggregation or accumulation of sheet thickness, thus leading to an ultrahigh surface area of  $371 \text{ m}^2 \text{ g}^{-1}$  ever obtained for  $\text{CoO}_x$  (Figure 6b, c). At the micro-scale, these few-layered  $\text{CoO}_x$  nanosheets were assembled into a large 3D, porous framework of nanotubes, which allowed for efficient charge and ion transport. Using this 2D/1D  $\text{CoO}_x$  heterostructure as an OER catalyst, a low onset potential of  $\approx 1.46 \text{ V}$  vs. RHE was achieved, and the current density was increased to  $51.2 \text{ mA cm}^{-2}$  at 1.65 V vs. RHE (Figure 6d, e). Furthermore, by coupling this 2D/1D  $\text{CoO}_x$  heterostructure and a Pt-mesh as the anode and cathode, respectively, a full water splitting

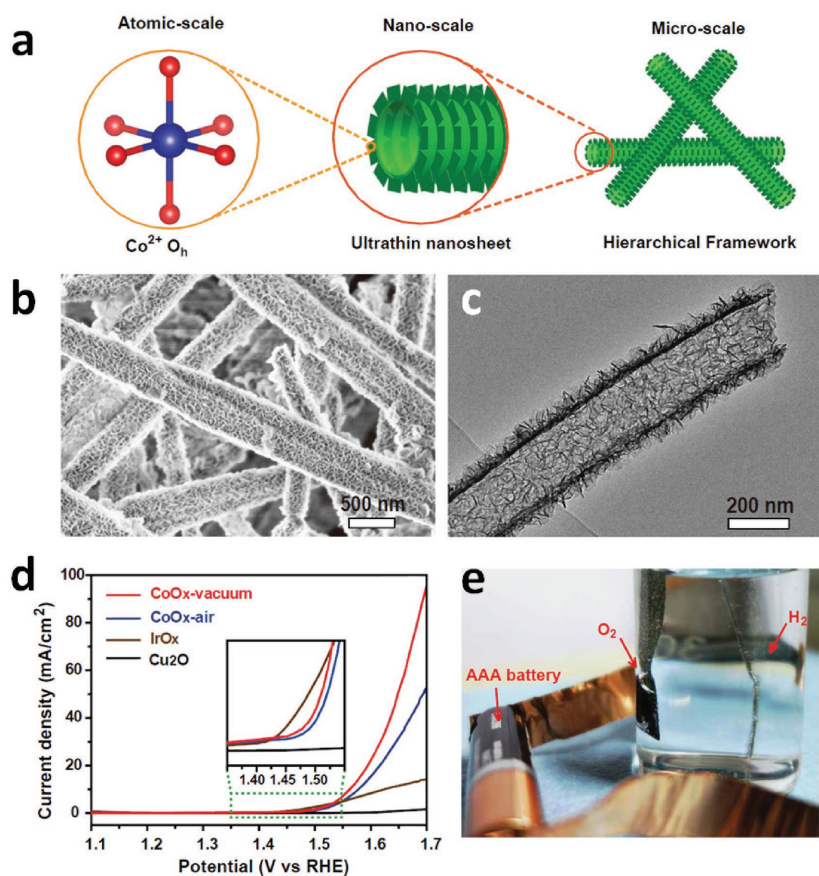


**Figure 6.** a) Schematic illustration of design of the hierarchical  $\text{CoO}_x$  nanosheet/nanotube structures with multiple scale optimizations. b) SEM and c) TEM images of the hierarchical  $\text{CoO}_x$  nanosheet/nanotube structures. d) Water oxidation current of the  $\text{CoO}_x$ -vacuum (red curve),  $\text{CoO}_x$ -air (blue curve),  $\text{IrO}_x$  (brown curve), and  $\text{Cu}_2\text{O}$  nanowire (black curve) at  $5 \text{ mV s}^{-1}$ . Inset: the zoom-in plot of the onset potential region. e) Demonstration of water splitting cell powered by a 1.5-V AAA battery. The  $\text{CoO}_x$  catalyst was loaded on Ni foam with a loading mass of  $4 \text{ mg cm}^{-2}$  as an anode and a Pt-mesh was used as a cathode. Reproduced with permission.<sup>[78]</sup>



electrolyzer was demonstrated using a single 1.5 V AAA alkaline battery, with a stable current density of  $\approx 1 \text{ mA cm}^{-2}$  for over 2 h.<sup>[78]</sup> Later, our group further developed the synthetic process by extending this growth strategy to a variety of 1D transition metal oxide structures such as  $\text{MnO}_x$ ,  $\text{ZnO}_x$ ,  $\text{NiO}_x$ ,  $\text{FeO}_x$ ,<sup>[79]</sup> and mixed Co-Ni hydroxides, as well as direct growth of these 1D nanostructures on conductive substrates.<sup>[80]</sup> These transition metal-based oxides and (oxy)hydroxides featured excellent OER activities, which were attributed to their abundant electrochemically reactive surface sites, 1D morphology for fast charge transport, and direct electrical contact to the underlying current collectors.

### 3.2. Incorporation of Metal-Based Nanomaterials on 1D Substrates

In addition to 1D morphologies of metal compounds, these metal-based catalysts can also be loaded onto different types of 1D conducting substrates to obtain the optimal performance. This design strategy is similar to the aforementioned incorporation of these metal-based nanomaterials on 1D substrates for HER catalysts. Thus, here we only specify some representative examples. For instance, a conducting network of copper nanowires was used to be electrodeposited with a conformal layer of nickel or cobalt around the nanowires, which was used as water oxidation catalyst.<sup>[81]</sup> A unique sandwich-like, 3D coaxial structure of Ni nanotube array coated with Ni and Co co-hydroxide nanosheets was demonstrated,<sup>[82]</sup> which featured both high surface area and enhanced electron transport. Nitrogen-doped

CNTs were also used to incorporate with spinel Mn-Co oxide nanoparticles by oxidative thermal scission.<sup>[83]</sup> During this process, the N-doped CNTs were ruptured, and the partially embedded Mn and Co nanoparticle catalysts were oxidized, with intimate contact to the graphene walls of CNTs. Recently, our group also demonstrated the conversion of a biomass, egg-shell membrane, into 3D grid-like fibrous carbon microstructures with abundant macropores, which were used for the growth of  $\text{NiCo}_2\text{O}_4$  nanowire arrays for efficient water oxidation.<sup>[84]</sup>

### 3.3. Metal-Free 1D Nanomaterials

Similar to HER, the metal-free OER catalyst has also been explored recently, in which CNTs or N-doped CNTs are the most extensively studied for 1D structures. In 2014, Tian et al. reported the synthesis of N-doped carbon coaxial nanocables, in which pristine CNTs and N-doped carbon layers were served as the core and shell (Figure 7a).<sup>[85]</sup> This coaxial 1D nanostructure allowed the enrichment of nitrogen atoms on the surface as well as the intact inner carbon walls, rendering a high electrical conductivity of  $3.3 \text{ S cm}^{-1}$  and a much enhanced OER activity for the catalyst. It was also reported that the surface of multiwalled CNTs could be tuned into an OER catalyst by mild surface oxidation, hydrothermal annealing and electrochemical activation (Figure 7b).<sup>[86]</sup> The catalytic mechanism was ascribed to the generation of oxygen-containing functional groups such as ketonic  $\text{C}=\text{O}$  on the outer walls of CNTs, which altered the electronic structures of adjacent carbon atoms and facilitated the adsorption of OER intermediates.

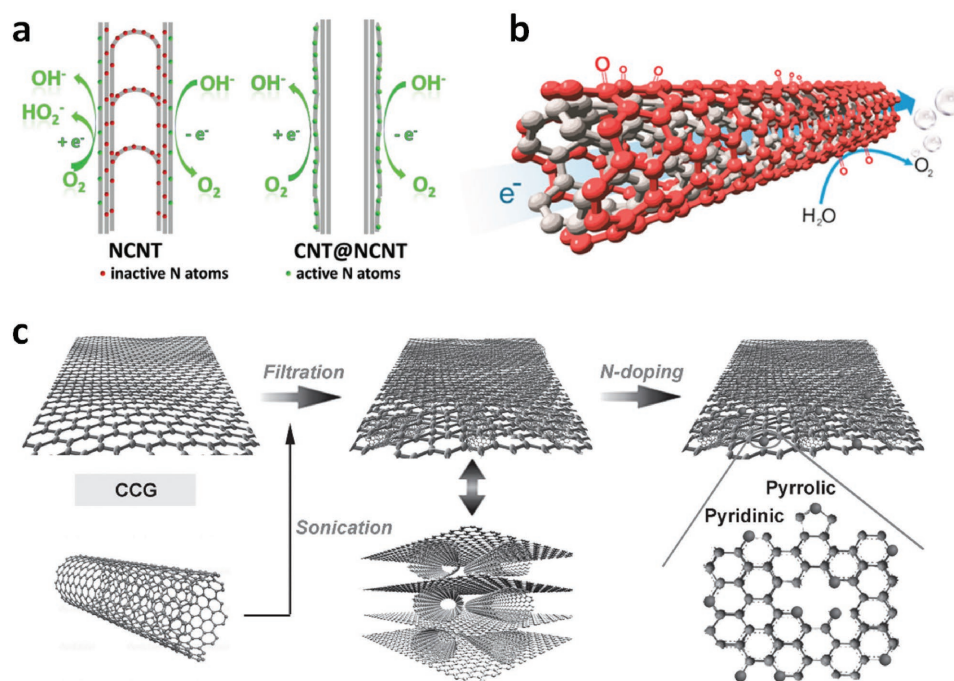


**Figure 7.** a) Schematic of the full exposure of active sites on the surface: NCNTs with bulk doping of nitrogen atoms, while CNT@NCNT coaxial nanocables with surface enriched nitrogen for OER. Reproduced with permission.<sup>[85]</sup> b) Schematic of the generation of oxygen-containing functional groups on the surface of CNTs. Reproduced with permission.<sup>[86]</sup> Copyright 2015, American Chemical Society. c) Schematic of the layer-by-layer synthetic process of NG-CNT. Reproduced with permission.<sup>[55]</sup>

In addition to single carbon structures, Qiao and coworkers reported the dual doping of nitrogen and oxygen on graphene-CNT hydrogel film,<sup>[55]</sup> via a layer-by-layer assembly of CNTs and graphene (with intrinsic oxygen impurities) through a simple filtration method, followed by annealing in ammoniac for nitrogen doping (Figure 7c). The high OER activity of this hybrid catalyst was attributed to the dual active sites originating from the chemically converted CNTs and graphene. Recently, our group reported the growth of a heterostructure of C<sub>3</sub>N<sub>4</sub>/CNTs/carbon fiber.<sup>[87]</sup> The OER performance was owing to the high nitrogen content of C<sub>3</sub>N<sub>4</sub> and the enhanced charge transport capability of the 1D/3D hierarchical carbon networks.

#### 4. Bifunctional HER/OER Catalyst

As described above, a number of earth-abundant non-noble materials have been investigated and developed in the past years as separate HER and OER catalysts, with substantial progresses of improving both the catalytic performances and long-time stability. Nonetheless, the HER catalysts such as transition metal sulfides, selenides and phosphides still function the best in acidic media, while the OER catalysts generally need to be used in alkaline conditions to avoid material dissolution.<sup>[10]</sup> The use of separate electrolytes (as well as separation films) within the same electrolyzer inevitably reduces the cell efficiency while at the same time increases the fabrication cost. Thus, the capability of preparing single materials that allow for both HER and OER in the same electrolyte represents a significant merit, not only for optimizing the conversion efficiency but also for large-scale and cost-effective deployment. In the past few years, a quick increase of research focus has been realized and dedicated to this field, with the efforts generally divided into two directions: (1) developing homologous material pairs that can be converted for HER and OER, respectively; and (2) exploring new materials/structures that are efficient for both HER and OER simultaneously.

##### 4.1. Homologous Material Pairs

One of the earliest demonstrations of the non-noble-metal bifunctional HER/OER electrocatalysts, although not in 1D morphologies, was reported by the Artero group in 2012.<sup>[88]</sup> In their work, a nanoparticulate material, namely H<sub>2</sub>-CoCat, was electrochemically synthesized from cobalt salts in a phosphate buffer solution. This new material was composed of metallic cobalt coated with a cobalt-oxo/hydroxo-phosphate layer, which allowed for hydrogen production from neutral buffer. Further electrochemical equilibration converted this H<sub>2</sub>-CoCat into a new form of amorphous cobalt oxide film, namely O<sub>2</sub>-CoCat that enabled O<sub>2</sub> evolution. It was found that the switching between these two material forms was reversible, which was also well correlated with the conversion of the morphologies at the electrode surface and two types of non-metallic atomic structures. Nonetheless, the catalytic properties of these early works were still far from optimum. Later, using a similar synthetic approach, Yu et al. demonstrated that by direct electrodepositing a Ni-based bifunctional material on 1D multiwalled

CNTs, the performance of the electrocatalytic activity was much improved.<sup>[89]</sup> Spectroscopic studies revealed that the content of oxygen in the O<sub>2</sub>-NiO<sub>x</sub>-CNT film (i.e., the OER catalyst) was higher than that in the H<sub>2</sub>-NiO<sub>x</sub>-CNT film (i.e., the HER catalyst). The Faradaic efficiencies for hydrogen and oxygen production were over 95%.

The chemical conversion between OER and HER catalysts using sulfidation or phosphidation has also been investigated. For example, Peng et al. reported the conversion of spinel-type NiCo<sub>2</sub>O<sub>4</sub> nanowires to pyrite-type Ni<sub>0.33</sub>Co<sub>0.67</sub>S<sub>2</sub> nanowires by sulfurization, which functioned as HER and OER catalysts, respectively.<sup>[35]</sup> A water splitting electrolyzer using these all-nanowire-based catalysts achieved a current density of 5 mA cm<sup>-2</sup> at 1.65 V. Similarly, Li et al. demonstrated the conversion of Co-Ni hydroxide nanowires into Co-Ni nitride nanowires by nitridation.<sup>[80]</sup> By using these Co-Ni hydroxide and nitride nanowires as anode and cathode, a current density of > 10 mA cm<sup>-2</sup> was obtained at 1.65 V. Although these water splitting experiments were carried out in the same electrolyte, it still requires extra steps for conversion between two material forms and thus increases complexity and cost.

##### 4.2. Single Nanostructure for HER and OER

The single composite of bifunctional electrocatalyst was first studied with metal components. In 2014, the Bao group reported the preparation of cobalt nanoparticles encapsulated in N-doped carbon (designated as Co@N-C), which displayed good HER performance in a wide pH range and OER performance in alkaline solution.<sup>[90]</sup> The applied potentials for Co@N-C in alkaline condition (1 M KOH) for HER and OER were measured as 0.33 and 1.63 V, in order to achieve current densities of 10 mA cm<sup>-2</sup>. These results were better than iron nanoparticles encapsulated in N-doped CNTs with similar nitrogen doping level. For the full electrolyzer using this Co@N-C as cathode and anode, a current density of ≈ 40 mA cm<sup>-2</sup> was obtained at an applied bias of 1.7 V.

In addition to serve as a conducting substrate, CNTs were also explored as templates for synthesize 1D nanostructures. The Leonard group prepared 1D nanocrystalline Mo<sub>2</sub>C using multiwalled CNTs as templates.<sup>[91]</sup> Although it was known that Mo<sub>2</sub>C could serve as a HER catalyst, its capability for OER had not been reported before. Using four different synthetic methods, the authors examined the electrocatalytic activities of these four products for HER in acid and alkaline electrolytes as well as OER in alkaline media. It was found out that 1D Mo<sub>2</sub>C nanostructures prepared with CNT templates presented the best performance among these four products, suggesting the virtues of 1D structures. Later, Tian et al. used a template-assisted electrodeposition method to synthesize a NiMo-alloy hollow nanorod array.<sup>[92]</sup> To obtain 10 mA cm<sup>-2</sup> current densities for HER and OER, overpotentials of 92 and 310 mV were required for the NiMo nanorod array, respectively. At an applied voltage of 1.64 V, this bifunctional electrocatalyst enabled an alkaline electrolyzer with 10 mA cm<sup>-2</sup>.

Chalcogenides are the most extensively approached targets for bifunctional electrocatalyst. For example, CoSe<sub>2</sub> is a well-known earth-abundant electrocatalyst, with two possible

crystalline phases, the orthorhombic macarsite-type (*o*-CoSe<sub>2</sub>) and the cubic pyrite-type (*c*-CoSe<sub>2</sub>) structures. However, previous studies only focused on the acidic HER activity or the alkaline OER activity of CoSe<sub>2</sub>. Wu, Xie and coworkers recently reported the phase transformation strategy and controlled synthesis of these two different CoSe<sub>2</sub> phases.<sup>[93]</sup> Density functional theory calculations showed the HER free energy change and water adsorption energy for the *o*-CoSe<sub>2</sub> and *c*-CoSe<sub>2</sub> products (Figure 8a). It was found out that under alkaline conditions, the *c*-CoSe<sub>2</sub> catalyst exhibited optimal water adsorption energy (Figure 8b), higher electrical conductivity (Figure 8c), and quicker kinetics and efficiency transforming the adsorbed hydrogen into H<sub>2</sub>, thus leading to better HER electrocatalytic activity over *o*-CoSe<sub>2</sub>. An alkaline water splitting electrolyzer based on this *c*-CoSe<sub>2</sub> catalyst showed a current density of 10 mA cm<sup>-2</sup> under 1.63 V, with excellent stability over 10,000 seconds (Figure 8d).

In 2015, the Sun group demonstrated the synthesis of NiSe nanowire film on nickel foam by a *in situ* hydrothermal method, using nickel foam and NaHSe as Ni and Se sources, respectively.<sup>[94]</sup> This NiSe nanowire grown on Ni foam behaved as a 3D electrode for both HER and OER in strongly alkaline media, with superior catalytic activity and durability. A cell voltage of 1.63 V was needed to drive the water electrolyzer to achieve 10 mA cm<sup>-2</sup>. The same group also reported the conversion of NiCo<sub>2</sub>O<sub>4</sub> nanowires on carbon cloth into NiCo<sub>2</sub>S<sub>4</sub> nanowires,<sup>[95]</sup> where the latter enabled 10 mA cm<sup>-2</sup> current density for full water splitting at a cell voltage of 1.68 V, which was 300 mV

lower than that for NiCo<sub>2</sub>O<sub>4</sub> under the same condition. Sivanantham et al. showed the direct growth of 1D NiCo<sub>2</sub>S<sub>4</sub> nanowire arrays on 3D Ni foam, which delivered 10 mA cm<sup>-2</sup> under a cell voltage of 1.63 V in an alkaline electrolyzer.<sup>[96]</sup> Other sulfides, selenides, phosphides and nitrides, including Ni-doped CoS<sub>2</sub> nanowires,<sup>[97]</sup> Ni<sub>3</sub>Se<sub>2</sub> nanoforests,<sup>[98]</sup> mesoporous CoP nanorod arrays,<sup>[99]</sup> hierarchical TiN@Ni<sub>3</sub>N nanowire arrays,<sup>[100]</sup> have also been reported.

Although oxides are typically known with good OER activity but not for HER, their potential for hydrogen evolution has also been investigated recently. The combination of oxides with graphitic carbon materials has been demonstrated as bifunctional catalysts, as the metal oxides and graphitic carbon materials can contribute each own strength for OER and HER, respectively, as previously reported by Co-Mn complex oxide superlattice coated by N-doped carbon conjugate.<sup>[23]</sup> Recently, Tahir et al. reported a facile, large-scale chemical synthesis of Co<sub>3</sub>O<sub>4</sub> embedded 1D tubular nanostructures of graphitic carbon nitride, which exhibited strong synergistic effect between Co<sub>3</sub>O<sub>4</sub> and graphitic carbon nitride.<sup>[101]</sup> This hybrid conjugate showed the lowest overpotential of 0.12 V for OER (Figure 9a), even smaller than RuO<sub>2</sub> (0.14 V) and IrO<sub>2</sub> (0.16 V). For HER, the composite presented a small onset of -0.03 V in 0.5 M H<sub>2</sub>SO<sub>4</sub> (Figure 9b), close to that of commercial Pt/C (-0.01 V). As the onset potential of plain graphitic carbon nitride was -0.27 V, it was concluded that the co-existence of Co<sub>3</sub>O<sub>4</sub> was beneficial for the HER performance. However, the HER and OER experiments in this work were not carried out

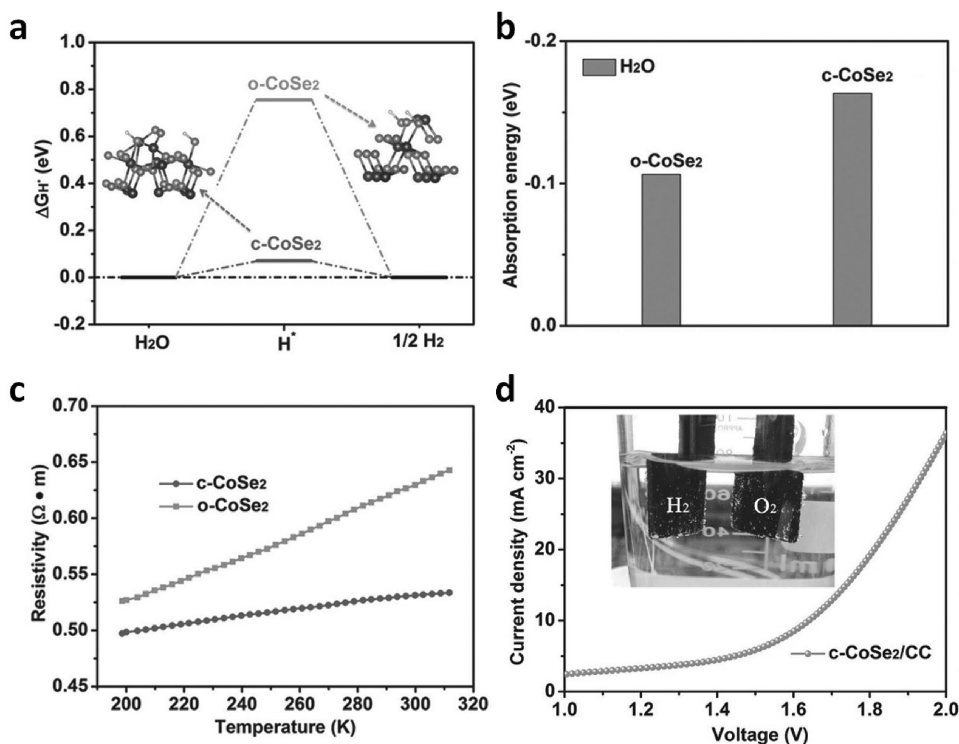


**Figure 8.** a) Calculated HER free-energy change and b) water adsorption energy for the *o*-CoSe<sub>2</sub> and *c*-CoSe<sub>2</sub> products. c) Temperature-dependent resistivity of simple *o*-CoSe<sub>2</sub> and *c*-CoSe<sub>2</sub> products. d) Polarization curve of water electrolysis using *c*-CoSe<sub>2</sub>/carbon cloth as both HER and OER electrocatalysts in a two-electrode configuration with a scan rate of 10 mV s<sup>-1</sup>. Inset: Optical photograph showing the generation of H<sub>2</sub> and O<sub>2</sub> bubbles on the *c*-CoSe<sub>2</sub>/carbon cloth electrode. Reproduced with permission.<sup>[93]</sup>

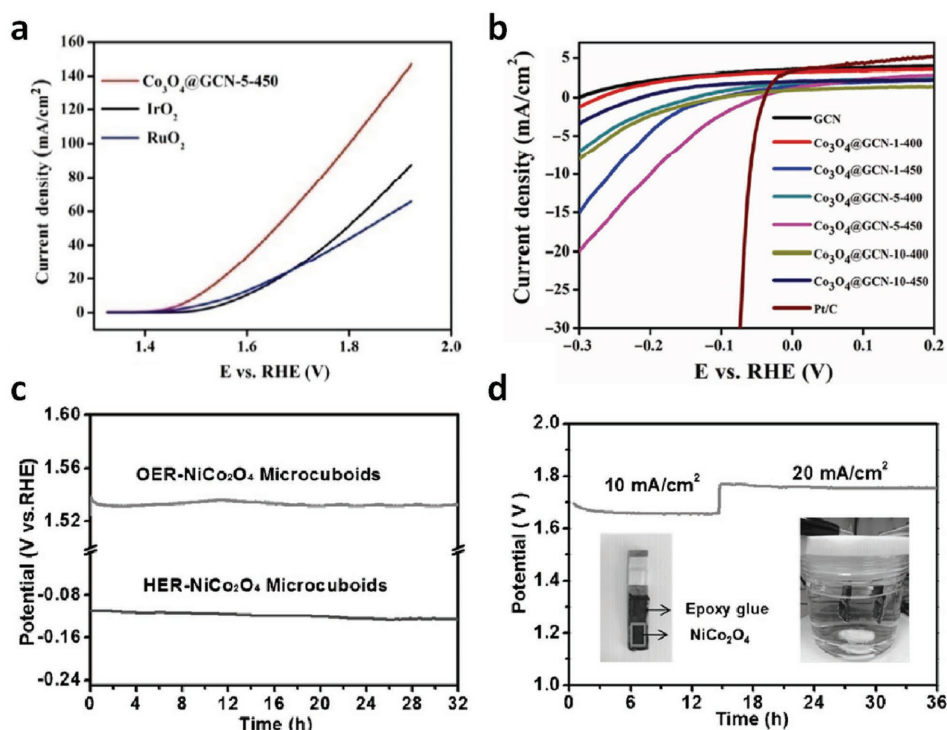


**Figure 9.** a) LSV curves of the  $\text{Co}_3\text{O}_4$ @GCN hybrid,  $\text{IrO}_2$ , and  $\text{RuO}_2$  at 1,600 rpm in 1 M KOH for OER. b) LSV curves of all samples and Pt/C at 1,600 rpm in 0.5 M  $\text{H}_2\text{SO}_4$  for HER. Reproduced with permission.<sup>[101]</sup> Copyright 2015, Springer. c) Galvanostatic measurement of OER and HER by  $\text{NiCo}_2\text{O}_4$  hollow microcuboids in 1 M NaOH at a current density of 10 and  $-10 \text{ mA cm}^{-2}$ , respectively. d) Overall water-splitting characteristics in a two-electrode configuration at current densities of 10 and  $20 \text{ mA cm}^{-2}$ . Inset in (b) shows optical image of  $\text{NiCo}_2\text{O}_4$  electrode and overall water-splitting device. Reproduced with permission.<sup>[102]</sup>

under the same pH conditions, and thus the full water splitting was not demonstrated. The mechanism of the synergistic effect between  $\text{Co}_3\text{O}_4$  and graphitic carbon nitride was still not fully understood. More recently, Gao et al. demonstrated that an unconventional, hierarchical  $\text{NiCo}_2\text{O}_4$  hollow microcuboids, consisting of 1D nanowires, were synthesized and used as good HER catalyst.<sup>[102]</sup> In 1 M KOH solution, the onset potential for HER was measured as  $-50 \text{ mV}$ . The overpotentials for driving cathodic current densities of 10 and  $100 \text{ mA cm}^{-2}$  were  $-110$  and  $-245 \text{ mV}$ , respectively (Figure 9c). For the overall water splitting, the current densities reached 10 and  $20 \text{ mA cm}^{-2}$  at applied potentials of 1.65 and 1.74 V, respectively (Figure 9d). These results were much better than those of  $\text{NiCo}_2\text{O}_4$  with microflower morphology, thus suggesting the importance of structural effect on water splitting performance.

## 5. Conclusion

In the past decade, the research community has been witnessing a substantial burst of interest and effort in searching new electrocatalysts for water splitting, with exquisite developments of controlling the synthesis of new materials/composites and the fabrication of new water splitting devices/systems. Due to the well-known limitation in using noble metal-based materials, it has been widely recognized that highly active and robust electrocatalysts, made of earth-abundant materials with low cost and good sustainability, are indispensable for realizing scalable

water splitting with high efficiency and excellent stability. In addition, it has also been well envisioned that nanoscale materials such as 1D nanostructures can bring significant benefits for achieving high apparent electrocatalytic activity for practical applications, which are generally attributed to the following features. First, the electrochemically active surface area of these 1D nanostructures can be substantially enhanced compared to their thin film or conjugate counterparts, resulting in more surface reaction capability. Second, the electrical conductivities of these 1D nanostructures can be well optimized due to their increased crystalline and reduced grain boundaries, thus enhancing the charge transport and transfer processes. Further introducing of additional conducting agents/substrates such as metal or carbon into the composite can further expedite the charge transport along these materials. Third, due to the interspacing between their adjacent neighbors, the mass transfer of electroactive reactants or products can be much enhanced, especially towards the deep portion of the aligned 1D nanostructure arrays, which are clearly advantageous than their bulk or thin film counterparts.

This review has introduced the recent progresses in designing and developing 1D earth-abundant nanomaterials/nanostructures as active HER or OER catalysts, with a brief summary of their preparation methods and electrocatalytic performances for water splitting. In spite of these achievements in developing low-cost catalysts, the research and investigation are still at an early stage. Several significant challenges exist, for both 1D nanomaterials and other structures, and need to be

solved in order to reach the next-stage milestones for catalytic water splitting with higher efficiency and stability.

First of all, the mechanism of water splitting with electrocatalysts needs to be further elucidated. The understanding of the mechanism of different HER, OER and bifunctional catalysts is not only important from fundamental science point of view, but also suggests potential directions for optimization of current catalyst behaviors as well as further rational design/synthesis of new materials for catalyst candidates. Although substantial studies have been carried out in investigating the structure-function inter-relationship of various catalysts with corresponding activity and stability, there is still lack of in-depth mechanistic investigation on an atomic level. The HER process for Pt under acidic conditions is relatively understood, but remains quite ambiguous under basic conditions especially for those composite materials. For OER and bifunctional catalysts, the knowledge of their working mechanisms towards water splitting is still preliminary. In particular, the fundamental studies on the electrochemical properties, electron-transfer behavior and multiple-electron coupled reaction mechanism are quite limited. Thus, a close integration of both advanced in situ characterization techniques and theoretical simulations is necessary to clarify the catalytic mechanism and advance the field.

Second, the development of new electrocatalytic materials nowadays has still largely depended on pre-requisite knowledge of existing materials and trial-and-errors, but very few materials have been discovered based the rational design and fundamental understanding the catalytic mechanism and the targeted electrochemical reactions.<sup>[17]</sup> Most of the works in this field have been focused on the observed electrochemical properties of these catalysts such as values of overpotentials and Tafel slopes, but the fundamental nature of these properties has largely been missing, which limit the capability of realizing new materials with significantly improved performances. For example, the bifunctional earth-abundant catalysts reported to date are all based on alkaline electrolyzers, which require additional gas separation steps. The bifunctional catalysts that can be stable in acidic conditions have not been discovered yet. The in-depth understanding of these features can surely expedite the material screening process, and may further point to new elements or composites that have not been studied for this application. In addition, although based on some simplified models, the DFT calculations are capable of providing a reasonably high level of accuracy to evaluate experimental data and predict potential directions.

Moreover, the comparison and leverage of different works are still difficult. For instance, the measurement and evaluation methods reported nowadays are not standardized so that it is difficult to compare results reported by different people/methods.<sup>[15]</sup> Particularly, the electrochemical performances reported in most of the studies are only normalized to the superficial geometric electrode area, but the specific surface morphology, effective surface area, as well as the catalyst loading quantity are either ignored or not aligned to make effective comparison. In addition, it is known that the nanocrystals with high-indexed facets can have much improved catalytic activity, while the realization of these high-indexed facets in low-dimensional (e.g. 1D and 2D) structures is still

substantially challenging. Thus, the design and optimization of those new catalysts should be in a large span of length scales, from atomic, nanoscale, to micro- and even macroscopic levels. The aims of these designs are to achieve the minimum free energy change for the reaction pathway on a given surface, while at the same time to optimize the effective surface area/sites for electrochemical reactions. In addition, the measurement methods should also be standardized and evaluated by third-parties to get valuable comparison across different results.

Last but not least, the capabilities of interfacing these electrocatalysts with semiconductor or molecular photoabsorbers, as well as large-scale synthesis and implementation of these electrocatalytic or photo-electrocatalytic materials, have yet to be demonstrated. The ultimate efficiency of the photoconversion system is determined by the nanoscale interfacial properties between semiconductor photoabsorbers and electrocatalysts, and thus the understanding and perfect control of these interfaces with exquisite tuning of charge separation and transfer are critical. In addition, the scale-up of synthesis and utilization of these catalyst materials with controlled size, morphology, composition and electrochemical properties need to be established. It should be aware that even though earth-abundant materials are used as low-cost precursors, the synthetic routes of these materials may not be cost effective or hard to be implemented in large scales. The total cost of the whole synthesis and electrochemical process, including the control of waste and acid/base pollution, should be carefully put into consideration and well optimized, in order to realize efficient and robust deployment of large-scale water splitting for sustainable energy requirement globally.

## Acknowledgements

We thank the following funding agencies for supporting this work: the National Key Basic Research Program of China (2013CB934104), the Natural Science Foundation of China (21322311, 21473038), the Science and Technology Commission of Shanghai Municipality (14JC1490500), the Program for Professor of Special Appointment (Eastern Scholar) at Shanghai Institutions of Higher Learning, and the Collaborative Innovation Center of Chemistry for Energy Materials (2011-iChem). J.L. specially thanks all the support of Fudan Undergraduate Research Opportunities Programs in the past four years, including Deng-Hui Program, Wang-Dao Program, and Hui-Chun Chin and Tsung-Dao Lee Chinese Undergraduate Research Endowment.

Received: September 22, 2016

Revised: October 25, 2016

Published online: December 27, 2016

- [1] M. G. Walter, E. L. Warren, J. R. McKone, S. W. Boettcher, Q. X. Mi, E. A. Santori, N. S. Lewis, *Chem. Rev.* **2010**, *110*, 6446.
- [2] C. Liu, B. C. Colon, M. Ziesack, P. A. Silver, D. G. Nocera, *Science* **2016**, *352*, 1210.
- [3] J. Luo, J. H. Im, M. T. Mayer, M. Schreier, M. K. Nazeeruddin, N. G. Park, S. D. Tilley, H. J. Fan, M. Gratzel, *Science* **2014**, *345*, 1593.
- [4] K. K. Sakimoto, A. B. Wong, P. D. Yang, *Science* **2016**, *351*, 74.
- [5] X. B. Chen, S. H. Shen, L. J. Guo, S. S. Mao, *Chem. Rev.* **2010**, *110*, 6503.

- [6] C. G. Morales-Guio, L. A. Stern, X. Hu, *Chem. Soc. Rev.* **2014**, *43*, 6555.
- [7] J. O. M. Bockris, *Int. J. Hydrogen Energy* **2013**, *38*, 2579.
- [8] Y. Jiao, Y. Zheng, M. Jaroniec, S. Z. Qiao, *Chem. Soc. Rev.* **2015**, *44*, 2060.
- [9] W. Kim, B. A. McClure, E. Edri, H. Frei, *Chem. Soc. Rev.* **2016**, *45*, 3221.
- [10] J. Ran, J. Zhang, J. Yu, M. Jaroniec, S. Z. Qiao, *Chem. Soc. Rev.* **2014**, *43*, 7787.
- [11] Y. Shi, B. Zhang, *Chem. Soc. Rev.* **2016**, *45*, 1529.
- [12] Y. Xu, M. Kraft, R. Xu, *Chem. Soc. Rev.* **2016**, *45*, 3039.
- [13] Y. Xu, B. Zhang, *Chem. Soc. Rev.* **2014**, *43*, 2439.
- [14] C. Ye, M. D. Regulacio, S. H. Lim, S. Li, Q. H. Xu, M. Y. Han, *Chem. Eur. J.* **2015**, *21*, 9514.
- [15] X. Zou, Y. Zhang, *Chem. Soc. Rev.* **2015**, *44*, 5148.
- [16] A. J. F. Bard, R. Larry, *Electrochemical Methods: Fundamentals and Applications*. John Wiley & Sons, Inc., New York, USA **2001**
- [17] M. S. Faber, S. Jin, *Energy Environ. Sci.* **2014**, *7*, 3519.
- [18] W. T. Hong, M. Risch, K. A. Stoerzinger, A. Grimaud, J. Suntivich, Y. Shao-Horn, *Energy Environ. Sci.* **2015**, *8*, 1404.
- [19] G. Wu, P. Zelenay, *Acc. Chem. Res.* **2013**, *46*, 1878.
- [20] S. J. Guo, S. Zhang, S. H. Sun, *Angew. Chem. Int. Ed.* **2013**, *52*, 8526.
- [21] M. Armand, J. M. Tarascon, *Nature* **2008**, *451*, 652.
- [22] L. Johnson, C. M. Li, Z. Liu, Y. H. Chen, S. A. Freunberger, P. C. Ashok, B. B. Praveen, K. Dholakia, J. M. Tarascon, P. G. Bruce, *Nat. Chem.* **2014**, *6*, 1091.
- [23] J. Li, Y. C. Wang, T. Zhou, H. Zhang, X. H. Sun, J. Tang, L. J. Zhang, A. M. Al-Enizi, Z. Q. Yang, G. F. Zheng, *J. Am. Chem. Soc.* **2015**, *137*, 14305.
- [24] J. Greeley, T. F. Jaramillo, J. Bonde, I. B. Chorkendorff, J. K. Nørskov, *Nat. Mater.* **2006**, *5*, 909.
- [25] J. Wang, W. Cui, Q. Liu, Z. Xing, A. M. Asiri, X. Sun, *Adv. Mater.* **2016**, *28*, 215.
- [26] Y. Li, P. Hasin, Y. Wu, *Adv. Mater.* **2010**, *22*, 1926.
- [27] M. S. Faber, R. Dziejczak, M. A. Lukowski, N. S. Kaiser, Q. Ding, S. Jin, *J. Am. Chem. Soc.* **2014**, *136*, 10053.
- [28] Y. L. Wang, T. Y. Wang, P. M. Da, M. Xu, H. Wu, G. F. Zheng, *Adv. Mater.* **2013**, *25*, 5177.
- [29] Y. D. Su, C. Liu, S. Brittan, J. Y. Tang, A. Fu, N. Kornienko, Q. Kong, P. D. Yang, *Nat. Nanotechnol.* **2016**, *11*, 609.
- [30] B. Tian, T. J. Kempa, C. M. Lieber, *Chem. Soc. Rev.* **2009**, *38*, 16.
- [31] T. J. Kempa, R. W. Day, S. K. Kim, H. G. Park, C. M. Lieber, *Energy Environ. Sci.* **2013**, *6*, 719.
- [32] H. Wu, Y. Cui, *Nano Today* **2012**, *7*, 414.
- [33] C. K. Chan, H. L. Peng, G. Liu, K. McIlwrath, X. F. Zhang, R. A. Huggins, Y. Cui, *Nat. Nanotechnol.* **2008**, *3*, 31.
- [34] A. I. Hochbaum, P. D. Yang, *Chem. Rev.* **2010**, *110*, 527.
- [35] Z. Peng, D. S. Jia, A. M. Al-Enizi, A. A. Elzatahry, G. F. Zheng, *Adv. Energy Mater.* **2015**, *5*, 1402031.
- [36] X. W. Liu, W. W. Li, H. Q. Yu, *Chem. Soc. Rev.* **2014**, *43*, 7718.
- [37] J. Tian, Q. Liu, A. M. Asiri, X. Sun, *J. Am. Chem. Soc.* **2014**, *136*, 7587.
- [38] P. Jiang, Q. Liu, Y. Liang, J. Tian, A. M. Asiri, X. Sun, *Angew. Chem. Int. Ed.* **2014**, *53*, 12855.
- [39] J. Tian, Q. Liu, N. Cheng, A. M. Asiri, X. Sun, *Angew. Chem. Int. Ed.* **2014**, *53*, 9577.
- [40] J. Tian, N. Cheng, Q. Liu, W. Xing, X. Sun, *Angew. Chem. Int. Ed.* **2015**, *54*, 5493.
- [41] Q. Ding, F. Meng, C. R. English, M. Caban-Acevedo, M. J. Shearer, D. Liang, A. S. Daniel, R. J. Hamers, S. Jin, *J. Am. Chem. Soc.* **2014**, *136*, 8504.
- [42] M. A. Lukowski, A. S. Daniel, F. Meng, A. Forticaux, L. Li, S. Jin, *J. Am. Chem. Soc.* **2013**, *135*, 10274.
- [43] J. Kibsgaard, Z. Chen, B. N. Reinecke, T. F. Jaramillo, *Nat. Mater.* **2012**, *11*, 963.
- [44] J. D. Benck, Z. Chen, L. Y. Kuritzky, A. J. Forman, T. F. Jaramillo, *ACS Catalysis* **2012**, *2*, 1916.
- [45] D. Voiry, H. Yamaguchi, J. Li, R. Silva, D. C. B. Alves, T. Fujita, M. Chen, T. Asefa, V. B. Shenoy, G. Eda, M. Chhowalla, *Nat. Mater.* **2013**, *12*, 850.
- [46] M. A. Lukowski, A. S. Daniel, C. R. English, F. Meng, A. Forticaux, R. J. Hamers, S. Jin, *Energy Environ. Sci.* **2014**, *7*, 2608.
- [47] E. J. Popczun, J. R. McKone, C. G. Read, A. J. Baciocchi, A. M. Wiltrout, N. S. Lewis, R. E. Schaak, *J. Am. Chem. Soc.* **2013**, *135*, 9267.
- [48] E. J. Popczun, C. G. Read, C. W. Roske, N. S. Lewis, R. E. Schaak, *Angew. Chem. Int. Ed.* **2014**, *53*, 5427.
- [49] J. R. McKone, B. F. Sadtler, C. A. Werlang, N. S. Lewis, H. B. Gray, *ACS Catalysis* **2013**, *3*, 166.
- [50] J. R. McKone, E. L. Warren, M. J. Bierman, S. W. Boettcher, B. S. Brunschwig, N. S. Lewis, H. B. Gray, *Energy Environ. Sci.* **2011**, *4*, 3573.
- [51] J. M. Wang, Y. M. Zheng, F. Q. Nie, J. Zhai, L. Jiang, *Langmuir* **2009**, *25*, 14129.
- [52] M. Caban-Acevedo, M. L. Stone, J. R. Schmidt, J. G. Thomas, Q. Ding, H. C. Chang, M. L. Tsai, J. H. He, S. Jin, *Nat. Mater.* **2015**, *14*, 1245.
- [53] W. F. Chen, J. T. Muckerman, E. Fujita, *Chem. Comm.* **2013**, *49*, 8896.
- [54] L. Liao, S. N. Wang, J. J. Xiao, X. J. Bian, Y. H. Zhang, M. D. Scanlon, X. L. Hu, Y. Tang, B. H. Liu, H. H. Girault, *Energy Environ. Sci.* **2014**, *7*, 387.
- [55] S. Chen, J. Duan, M. Jaroniec, S. Z. Qiao, *Adv. Mater.* **2014**, *26*, 2925.
- [56] M. Gong, W. Zhou, M. C. Tsai, J. Zhou, M. Guan, M. C. Lin, B. Zhang, Y. Hu, D. Y. Wang, J. Yang, S. J. Pennycook, B. J. Hwang, H. Dai, *Nat. Commun.* **2014**, *5*, 4695.
- [57] X. Zou, X. Huang, A. Goswami, R. Silva, B. R. Sathe, E. Mikmekova, T. Asefa, *Angew. Chem. Int. Ed.* **2014**, *126*, 4461.
- [58] D. J. Li, U. N. Maiti, J. Lim, D. S. Choi, W. J. Lee, Y. Oh, G. Y. Lee, S. O. Kim, *Nano Lett.* **2014**, *14*, 1228.
- [59] J. Deng, P. J. Ren, D. H. Deng, L. Yu, F. Yang, X. H. Bao, *Energy Environ. Sci.* **2014**, *7*, 1919.
- [60] Z. Xing, Q. Liu, W. Xing, A. M. Asiri, X. Sun, *ChemSusChem* **2015**, *8*, 1850.
- [61] Q. Liu, J. Tian, W. Cui, P. Jiang, N. Cheng, A. M. Asiri, X. Sun, *Angew. Chem. Int. Ed.* **2014**, *126*, 6828.
- [62] D. Y. Wang, M. Gong, H. L. Chou, C. J. Pan, H. A. Chen, Y. Wu, M. C. Lin, M. Guan, J. Yang, C. W. Chen, Y. L. Wang, B. J. Hwang, C. C. Chen, H. Dai, *J. Am. Chem. Soc.* **2015**, *137*, 1587.
- [63] W. Cui, Q. Liu, N. Cheng, A. M. Asiri, X. Sun, *Chem. Comm.* **2014**, *50*, 9340.
- [64] M. Shalom, S. Gimenez, F. Schipper, I. Herraiz-Cardona, J. Bisquert, M. Antonietti, *Angew. Chem. Int. Ed.* **2014**, *126*, 3728.
- [65] Y. Zheng, Y. Jiao, Y. Zhu, L. H. Li, Y. Han, Y. Chen, A. Du, M. Jaroniec, S. Z. Qiao, *Nat. Commun.* **2014**, *5*, 3783.
- [66] N. Holmberg, K. Laasonen, *J. Phys. Chem. C* **2015**, *119*, 16166.
- [67] N. Holmberg, K. Laasonen, *J. Phys. Chem. Lett.* **2015**, *6*, 3956.
- [68] Y. Matsumoto, E. Sato, *Mater. Chem. Phys.* **1986**, *14*, 397.
- [69] Y. Gorlin, T. F. Jaramillo, *J. Am. Chem. Soc.* **2010**, *132*, 13612.
- [70] W. J. Zhou, X. J. Wu, X. H. Cao, X. Huang, C. L. Tan, J. Tian, H. Liu, J. Y. Wang, H. Zhang, *Energy Environ. Sci.* **2013**, *6*, 2921.
- [71] I. Nikolov, R. Darkaoui, E. Zhecheva, R. Stoyanova, N. Dimitrov, T. Vitanov, *J. Electroanal. Chem.* **1997**, *429*, 157.
- [72] X. J. Liu, Z. Chang, L. Luo, T. H. Xu, X. D. Lei, J. F. Liu, X. M. Sun, *Chem. Mater.* **2014**, *26*, 1889.
- [73] Y. Wang, T. Zhou, K. Jiang, P. Da, Z. Peng, J. Tang, B. Kong, W.-B. Cai, Z. Yang, G. Zheng, *Adv. Energy Mater.* **2014**, *4*, 1400696.

- [74] X. B. Chen, L. Liu, P. Y. Yu, S. S. Mao, *Science* **2011**, 331, 746.
- [75] G. M. Wang, H. Y. Wang, Y. C. Ling, Y. C. Tang, X. Y. Yang, R. C. Fitzmorris, C. C. Wang, J. Z. Zhang, Y. Li, *Nano Lett.* **2011**, 11, 3026.
- [76] G. M. Wang, Y. C. Ling, H. Y. Wang, X. Y. Yang, C. C. Wang, J. Z. Zhang, Y. Li, *Energy Environ. Sci.* **2012**, 5, 6180.
- [77] Y. Meng, W. Song, H. Huang, Z. Ren, S. Y. Chen, S. L. Suib, *J. Am. Chem. Soc.* **2014**, 136, 11452.
- [78] Y. C. Wang, K. Jiang, H. Zhang, T. Zhou, J. W. Wang, W. Wei, Z. Q. Yang, X. H. Sun, W. B. Cai, G. F. Zheng, *Adv. Sci.* **2015**, 2, 1500003.
- [79] W. Wei, Y. C. Wang, H. Wu, A. M. Al-Enizi, L. J. Zhang, G. F. Zheng, *Nanotechnol.* **2016**, 27, LT201.
- [80] S. W. Li, Y. C. Wang, S. J. Peng, L. J. Zhang, A. M. Al-Enizi, H. Zhang, X. H. Sun, G. F. Zheng, *Adv. Energy Mater.* **2016**, 6, 1501661.
- [81] Z. Chen, A. R. Rathmell, S. Ye, A. R. Wilson, B. J. Wiley, *Angew. Chem. Int. Ed.* **2013**, 52, 13708.
- [82] Z. L. Zhao, H. X. Wu, H. L. He, X. L. Xu, Y. D. Jin, *Adv. Funct. Mater.* **2014**, 24, 4698.
- [83] A. Zhao, J. Masa, W. Xia, A. Maljusch, M. G. Willinger, G. Clavel, K. Xie, R. Schlogl, W. Schuhmann, M. Muhler, *J. Am. Chem. Soc.* **2014**, 136, 7551.
- [84] J. Geng, H. Wu, A. M. Al-Enizi, A. A. Elzatahry, G. Zheng, *Nanoscale* **2015**, 7, 14378.
- [85] G. L. Tian, Q. Zhang, B. S. Zhang, Y. G. Jin, J. Q. Huang, D. S. Su, F. Wei, *Adv. Funct. Mater.* **2014**, 24, 5956.
- [86] X. Lu, W. L. Yim, B. H. Suryanto, C. Zhao, *J. Am. Chem. Soc.* **2015**, 137, 2901.
- [87] Z. Peng, S. W. Yang, D. S. Jia, P. M. Da, P. He, A. M. Al-Enizi, G. Q. Ding, X. M. Xie, G. F. Zheng, *J. Mater. Chem. A* **2016**, 4, 12878.
- [88] S. Cobo, J. Heidkamp, P. A. Jacques, J. Fize, V. Fourmond, L. Guetaz, B. Jousselme, V. Ivanova, H. Dau, S. Palacin, M. Fontecave, V. Artero, *Nat. Mater.* **2012**, 11, 802.
- [89] X. Yu, T. Hua, X. Liu, Z. Yan, P. Xu, P. Du, *ACS Appl Mater Interfaces* **2014**, 6, 15395.
- [90] J. Wang, D. F. Gao, G. X. Wang, S. Miao, H. H. Wu, J. Y. Li, X. H. Bao, *J. Mater. Chem. A* **2014**, 2, 20067.
- [91] Y. N. Regmi, C. Wan, K. D. Duffee, B. M. Leonard, *ChemCatChem* **2015**, 7, 3911.
- [92] J. Q. Tian, N. Y. Cheng, Q. Liu, X. P. Sun, Y. Q. He, A. M. Asiri, *J. Mater. Chem. A* **2015**, 3, 20056.
- [93] P. Chen, K. Xu, S. Tao, T. Zhou, Y. Tong, H. Ding, L. Zhang, W. Chu, C. Wu, Y. Xie, *Adv. Mater.* **2016**, 28, 7527.
- [94] C. Tang, N. Cheng, Z. Pu, W. Xing, X. Sun, *Angew. Chem. Int. Ed.* **2015**, 54, 9351.
- [95] D. Liu, Q. Lu, Y. Luo, X. Sun, A. M. Asiri, *Nanoscale* **2015**, 7, 15122.
- [96] A. Sivanantham, P. Ganesan, S. Shanmugam, *Adv. Funct. Mater.* **2016**, 26, 4661.
- [97] W. Z. Fang, D. N. Liu, Q. Lu, X. P. Sun, A. M. Asiri, *Electrochem. Commun.* **2016**, 63, 60.
- [98] R. Xu, R. Wu, Y. M. Shi, J. F. Zhang, B. Zhang, *Nano Energy* **2016**, 24, 103.
- [99] Y. P. Zhu, Y. P. Liu, T. Z. Ren, Z. Y. Yuan, *Adv. Funct. Mater.* **2015**, 25, 7337.
- [100] Q. T. Zhang, Y. H. Wang, Y. C. Wang, A. M. Al-Enizi, A. A. Elzatahry, G. F. Zheng, *J. Mater. Chem. A* **2016**, 4, 5713.
- [101] M. Tahir, N. Mahmood, X. X. Zhang, T. Mahmood, F. K. Butt, I. Aslam, M. Tanveer, F. Idrees, S. Khalid, I. Shakir, Y. M. Yan, J. J. Zou, C. B. Cao, Y. L. Hou, *Nano Res.* **2015**, 8, 3725.
- [102] X. H. Gao, H. X. Zhang, Q. G. Li, X. G. Yu, Z. L. Hong, X. W. Zhang, C. D. Liang, Z. Lin, *Angew. Chem. Int. Ed.* **2016**, 128, 6398.